JGR Oceans

RESEARCH ARTICLE
10.1029/2024JC021679

Special Collection:
Regional Sea Level Change and Society

Influence of Ocean Model Horizontal Resolution on the Representation of Global Annual-To-Multidecadal Coastal Sea Level Variability

Christopher M. Little[1], Stephen G. Yeager[2], Rui M. Ponte[1], Ping Chang[3], and Who M. Kim[2]

[1]Atmospheric and Environmental Research, Lexington, MA, USA, [2]National Center for Atmospheric Research, Boulder, CO, USA, [3]Texas A&M University, Department of Oceanography, College Station, TX, USA

Key Points:

- While resolution-related improvements are pervasive, their magnitude and nature vary widely across coastal dynamic regimes
- Near western boundary currents, coastal sea level exhibits dramatic resolution-related increases in intrinsic variability
- Outside of eddy-rich regions, simulated coastal sea level variability is damped relative to observations, even at 0.1° resolution

Supporting Information:

Supporting Information may be found in the online version of this article.

Correspondence to:

C. M. Little,
clittle@aer.com

Citation:

Little, C. M., Yeager, S. G., Ponte, R. M., Chang, P., & Kim, W. M. (2024). Influence of ocean model horizontal resolution on the representation of global annual-to-multidecadal coastal sea level variability. *Journal of Geophysical Research: Oceans*, *129*, e2024JC021679. https://doi.org/10.1029/2024JC021679

Received 2 AUG 2024
Accepted 8 DEC 2024

Author Contributions:

Conceptualization: Christopher M. Little, Stephen G. Yeager, Ping Chang
Formal analysis: Christopher M. Little
Funding acquisition: Christopher M. Little, Stephen G. Yeager, Rui M. Ponte
Investigation: Christopher M. Little
Methodology: Christopher M. Little, Stephen G. Yeager, Who M. Kim
Resources: Christopher M. Little, Ping Chang, Who M. Kim
Visualization: Christopher M. Little
Writing – original draft: Christopher M. Little, Stephen G. Yeager, Rui M. Ponte

Abstract Emerging high-resolution global ocean climate models are expected to improve both hindcasts and forecasts of coastal sea level variability by better resolving ocean turbulence and other small-scale phenomena. To examine this hypothesis, we compare annual to multidecadal coastal sea level variability over the 1993–2018 period, as observed by tide gauges and as simulated by two identically forced ocean models, at ∼1° (LR) and ∼0.1° (HR) horizontal resolution. Differences between HR and LR, and misfits with tide gauges, are spatially coherent at regional alongcoast scales. Resolution-related improvements are largest in, and near, marginal seas. Near attached western boundary currents, sea level variance is several times greater in HR than LR, but correlations with observations may be reduced, due to intrinsic ocean variability. Globally, in HR simulations, intrinsic variability comprises from zero to over 80% of coastal sea level variance. Outside of eddy-rich regions, simulated coastal sea level variability is generally damped relative to observations. We hypothesize that weak coastal variability is related to large-scale, remotely forced, variability; in both HR and LR, tropical sea level variance is underestimated by ∼50% relative to satellite altimetric observations. Similar coastal dynamical regimes (e.g., attached western boundary currents) exhibit a consistent sensitivity to horizontal resolution, suggesting that these findings are generalizable to regions with limited coastal observations.

Plain Language Summary Recent advancements in global ocean climate models, particularly increases in horizontal resolution, are expected to improve predictions of coastal sea level changes. In this study, we compared sea level data recorded by tide gauges from 1993 to 2018 with Community Earth System Model (CESM) simulations at a lower (∼1°) and higher (∼0.1°) horizontal resolution. The higher-resolution model better represents the influence of small-scale turbulent ocean behavior. In some regions, turbulent ocean variability plays a significant role in coastal sea level changes, and can account for more than half of the variance. However, despite these improvements, simulated sea level changes remain smaller than observations in many regions, even at high model resolution. This underestimate of variability is apparent in CESM across much of the tropical oceans.

1. Introduction

Global ocean climate models (GOCMs), in both atmospherically forced and coupled configurations, are widely employed to: (a) understand and reconstruct drivers of variability and (b) make climate and sea level projections over seasonal to centennial timescales. To date, the horizontal resolution of GOCMs is generally on the order of 1°. At this resolution, GOCMs can not represent many processes known to govern coastal sea level variability (e.g., Becker et al., 2016; Holt et al., 2017; Penduff et al., 2010; Woodworth et al., 2019). For example, small-scale turbulence, generated only in models of sufficiently high resolution, introduces chaotic ("intrinsic") sea level variations at meso-to basin-scales (Close et al., 2020; Penduff et al., 2010; Sérazin et al., 2015). In addition, coastal regions are characterized by dramatic variations in bathymetry, and complex land boundaries that strongly influence ocean circulation. The presence of a continental slope damps and smooths sea level variability on continental shelves relative to the deep ocean, while coastal variability can be enhanced relative to, and/or decorrelated from, offshore locations, due to tightly coastally trapped signals (Gill, 1982; Hughes et al., 2019; Huthnance, 2004; Little et al., 2019; Roussenov et al., 2008; Vinogradov & Ponte, 2011; Wise et al., 2018, 2020; Woodworth et al., 2019). Collectively, these physical constraints drive a highly spatially variable sea level response to local and remote surface forcing that is often distinct from the open ocean.

Writing – review & editing: Christopher M. Little, Stephen G. Yeager, Rui M. Ponte, Ping Chang, Who M. Kim

Increases in GOCM horizontal resolution permit a more complete representation of forced and intrinsic ocean processes, and are thus expected to improve hindcasts and forecasts of coastal sea level variability. High-resolution regional and global simulations indicate that sea level is significantly influenced, and generally improved, by increased ocean model resolution (Chaigneau et al., 2022; Hermans et al., 2020; Li et al., 2022; Liu et al., 2016; Penduff et al., 2010; Tinker et al., 2020; van Westen et al., 2020; X. Zhang et al., 2017) (see also Figure 1) (A common threshold for "high resolution" is 0.1°, permitting explicit resolution of the first baroclinic deformation radius over most regions equatorward of ∼60° latitude (Hallberg, 2013)). Substantial resolution-sensitivity has been noted in forecasts over lead times ranging from seasonal to centennial (Hermans et al., 2020; Li et al., 2022; Liu et al., 2016; Long et al., 2021; Saba et al., 2016).

To improve confidence in sea level forecasts and understanding of resolution and/or parameterization requirements, it is vital to assess the representation of historical sea level variability, especially along coastlines, where: (a) human and ecosystem impacts are most evident (Cooley & Skern-Mauritzen, 2022; NOAA, 2022) and (b) tide gauges provide long observational records (Holgate et al., 2013). Potentially because of their coarse resolution, most efforts to assess the fidelity of global models have focused on large-scale sea level variability (e.g., Griffies et al., 2014; Tsujino et al., 2020), with fewer direct comparisons to individual tide gauges (e.g., Little et al., 2017). Previous evaluations of coastal sea level variability in high resolution models have had a regional focus (Chaigneau et al., 2022; Hermans et al., 2020; Li et al., 2022; Tinker et al., 2020; van Westen et al., 2020). Such results are not likely to be globally generalizable, as the importance of relevant physical processes varies on a regional basis (governed by their physical characteristics, nearby large-scale ocean circulation, and surface forcing) and as a function of timescale. There is also the less-discussed possibility for degraded agreement with observations at high resolution, even in forced simulations, due to increased ocean intrinsic variability.

Clean separation of intrinsic and forced variability, especially near coastlines, is not trivial, as it generally entails computationally intensive ensemble simulations, which are rarely performed with eddy-resolving ocean models. Previous studies (Carret et al., 2021; Close et al., 2020; Sérazin et al., 2015) have quantified the relative roles of intrinsic and forced variability based on a 50-member ensemble of global ocean-only model simulations using eddy-permitting 0.25° horizontal grids. These analyses show substantial contributions of intrinsic sea level variability across a variety of time scales and over vast areas of the global oceans, including western boundary currents. However, results have not been directly compared to tide gauge observations of coastal sea level. Furthermore, a 0.25° resolution may not be sufficient to capture all relevant processes and physical constraints. No previous analysis has quantified the relative roles of intrinsic and forced coastal sea level variability in a model of sufficiently high resolution to explicitly resolve midlatitude mesoscale turbulence.

Here, we conduct a global comparison of simulated coastal sea level variability and the tide gauge record using a set of paired high- (HR) and low- (LR) resolution forced ocean/sea-ice (FOSI) simulations performed using the Community Earth System Model (Chang et al., 2020). These simulations isolate the role of ocean model resolution and facilitate evaluation of both the amplitude and phasing of sea level variability. They also comprise an "ensemble of opportunity" facilitating an initial global assessment of the magnitude of oceanic intrinsic variability in coastal sea level.

2. Methods

2.1. CESM Simulations

We utilize sea surface height ("SSH"; equivalent to dynamic sea level (Gregory et al., 2019)) fields from global Community Earth System Model version 1.3 (CESM1.3) simulations at ∼0.1° (HR) and ∼1° (LR) horizontal resolution (Chang et al., 2020). The focus here is on forced ocean/sea-ice (FOSI) simulations using CESM1.3 (Small et al., 2024) that follow the Ocean Model Intercomparison Project version 2 (OMIP2) experimental protocol (Griffies et al., 2016). FOSI simulations utilize bias-corrected, reanalysis-based atmospheric data sets (e.g., Large & Yeager, 2009; Tsujino et al., 2018) to impart historical variability into the ocean and sea-ice components of climate models without the need for expensive data assimilation in those components. Since the advent of a coordinated experimental protocol (Griffies et al., 2009), the FOSI approach for reconstructing historical states has been widely adopted for comparative evaluations of ocean/sea-ice models and investigations of historical seasonal-to-decadal variability (e.g., Danabasoglu et al., 2014; Downes et al., 2015; Farneti et al., 2015; Ilıcak et al., 2016; Tseng et al., 2016; Wang et al., 2016). While FOSI experiments are now common and well-documented (thanks to their relative simplicity and economy) and permit state reconstruction from the

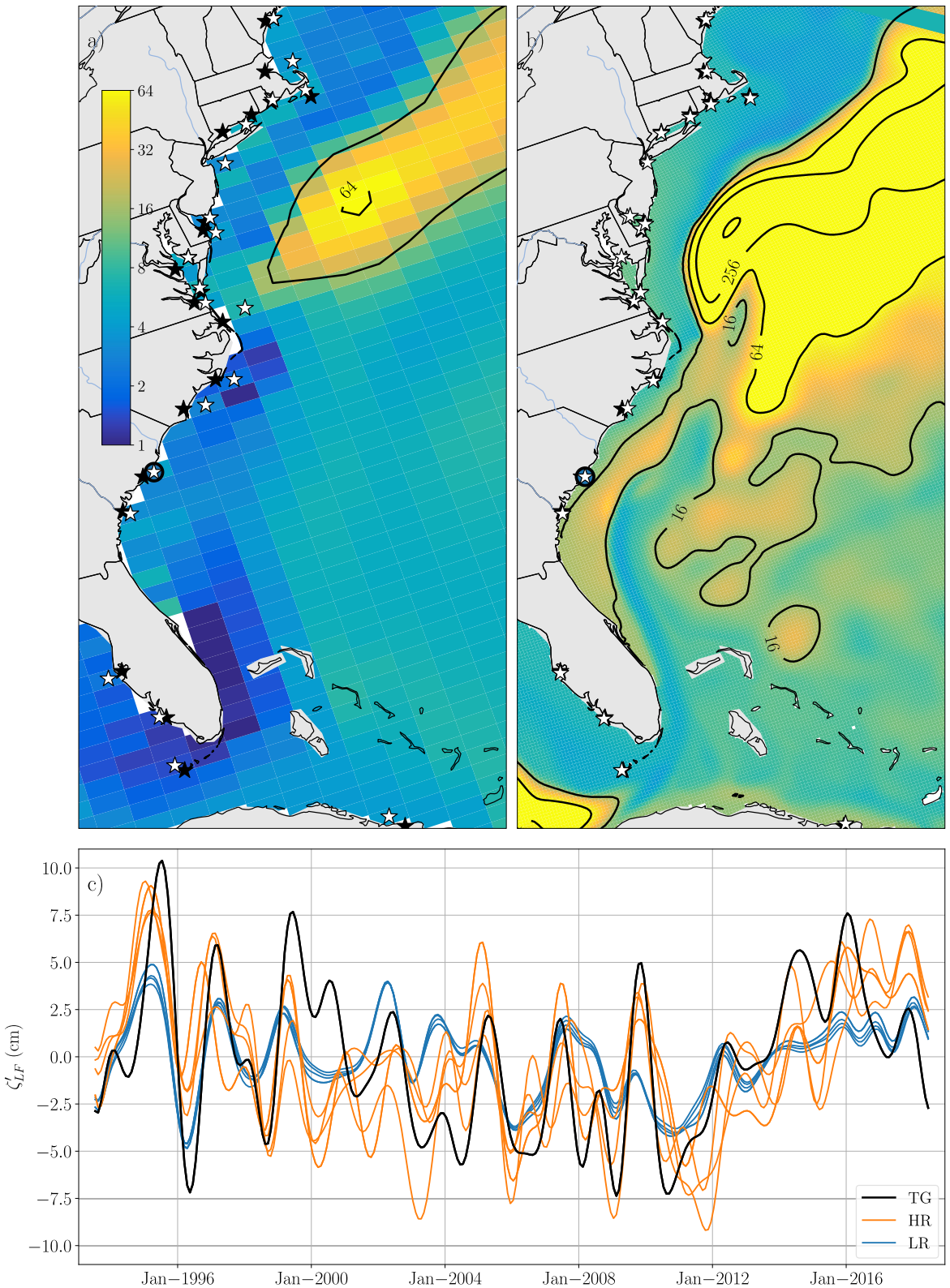
a)
64
32
16
8
4
2
1
64
b)
256
16
64
16
16
c)
10.0
7.5
5.0
2.5
0.0
−2.5
−5.0
−7.5
−10.0
ζ^t_{LF} (cm)
Jan−1996
Jan−2000
Jan−2004
Jan−2008
Jan−2012
Jan−2016
TG
HR
LR

Figure 1.

mid-twentieth century to near present, there are known issues with the experimental design (including spurious feedbacks, imperfect spin-up procedures, and uncertainties in the prescribed atmospheric state; see discussions in Griffies et al. (2009, 2016)) that limit the strength of conclusions that can be drawn from FOSI simulations. Nevertheless, FOSI state reconstruction has proven quite successful, if not optimal, for initializing seasonal to decadal climate predictions with the CESM model in both LR (Yeager et al., 2018, 2022) and HR (Yeager et al., 2023; Q. Zhang et al., 2024) configurations. It is likely that FOSI experimental design choices impact SSH state reconstruction (Griffies et al., 2014), but as the intent here is to present a baseline assessment of coastal sea level variability obtained in pre-existing CESM1.3 FOSIs at different resolutions, we leave an in-depth investigation of experimental design sensitivity for future work.

The OMIP2 protocol uses 1958–2018 forcing derived from JRA55 reanalysis (JRA55do; Tsujino et al., 2018) and represents the current state-of-the-art for FOSI model intercomparisons (Tsujino et al., 2020). Recent work has expanded OMIP2 evaluation to include HR configurations (e.g., Chassignet et al., 2020; Small et al., 2024), and this paper builds on those HR/LR comparisons with the aim of highlighting potential benefits of increased resolution under a given experimental design. In OMIP2, simulations are initialized from observed ocean/sea-ice climatology and spun up through consecutive cycles of 1958–2018 (61-year) forcing. Simulation years 62–122 (cycle 2) repeats the forcing of simulation years 1–61 (cycle 1), etc. The JRA55do atmospheric fields at ~55 km spatial resolution and 3-hr temporal resolution are interpolated to the HR (~10 km) and LR (~100 km) grids prior to surface flux computations.

While HR and LR FOSI simulations are subject to identical forcing fields, the horizontal grid differences are accompanied by a multitude of configuration differences (including bathymetry, parameterized physics, and tracer advection scheme (Chassignet et al., 2020)) that could contribute to simulation differences. For the purposes of this paper, "horizontal resolution" encompasses all model configuration choices that go along with the choice of a particular horizontal mesh.

We analyze monthly mean output from years 1993–2018 from cycles 1–4 (104 years of simulation for each model resolution). Since the forcing applied is (nearly) identical, cycle-to-cycle differences within each experiment can be attributed largely to intrinsic ocean variability.

In addition to FOSI simulations, we analyze a HR repeat-year-forcing (RYF) simulation conducted using repeat application of a single year of JRA55do boundary conditions (May 2003 to the end of April 2004) (Stewart et al., 2020). Deseasonalized monthly variability in the RYF simulation can also be attributed largely to intrinsic variability. Here, we use the last 26 years of monthly output from a 70-year RYF simulation.

2.2. Observational Data Sets, and Corrections Applied for Model-Data Comparison

We use monthly mean tide gauge records, retrieved from the Permanent Service for Mean Sea Level Revised Local Reference database on 1 December 2022 (Holgate et al., 2013; Permanent Service for Mean Sea Level, 2024), that have less than 12 missing months, in total, over the 1993–2018 period. Gaps in monthly records are filled after removal of the seasonal cycle and linear trend (see below) using linear interpolation. The initial data set of 365 tide gauge records provides reasonably dense spatial coverage over many coastlines (e.g., the continental United States, Europe, and Japan) but leaves significant gaps in other regions (e.g., most of the southern hemisphere).

Coastal sea level, as recorded by tide gauges, is influenced by several processes which are absent in CESM. These include the inverted barometer effect (IBE), global mean steric expansion/contraction, mass transfers from land and land-based ice to the ocean (barystatic changes), changes in the geoid, vertical land motion, and astronomical forcing (Gregory et al., 2019; Kopp et al., 2015). CESM simulations explicitly simulate only dynamic sea level (ζ)

Figure 1. Detrended, deseasonalized, 13-month low-passed coastal sea level $\left(\zeta'_{LF}\right)$ variance (in cm^2, on a $\log_2$ scale; see methods for processing details) over the 1993–2018 period, for the third forcing cycle of LR (a) and HR (b), calculated on each model's native grid. Both shading and contours represent variance; larger values are shown with contours where shading is saturated. Tide gauge locations are shown with black stars. Model grid points closest to tide gauge locations are shown with white stars. (c) ζ'_{LF} at the Charleston tide gauge (black), and for LR (blue) and HR (orange), at grid points closest to the tide gauge (circled stars in (a) and (b)). In (c), the four lines for LR and HR reflect forcing cycles 1–4. Inter-cycle differences arise from intrinsic variability (due to differences in initial conditions resulting from the cyclic forcing protocol).

variability, although the global mean steric component can be computed offline from density fields (Gregory et al., 2019).

We thus remove the following components from the tide gauge record, at monthly temporal resolution: global mean sea level due to barystatic and steric processes, using altimetry-derived estimates (MEaSUREs, 2021); and IBE, using surface pressure fields from the ERA-5 atmospheric reanalysis (Hersbach et al., 2020). The effect of these "corrections" is generally consistent with the single location shown in Figure 2: removal of IBE reduces variance predominantly over interannual timescales (see Supplementary Figure S1 in Supporting Information S1), with global mean corrections becoming increasingly more important at lower frequencies. We note that these corrections are not comprehensive, however, the effect of other unrepresented processes is expected to be small in most locations over the timescales considered here.

While trends in ζ are present in FOSI simulations, comparison with trends in the tide gauge record is ambiguous given local and regional signals (presumably largely due to vertical land motion) that are unrepresented in ocean models, and the potential influence of model drift. We thus linearly detrend both model ζ timeseries and "corrected" tide gauge time series; these trends are shown in Supplementary Figure S2 in Supporting Information S1. After correction and detrending, sea level in both CESM and tide gauges is denoted by ζ'.

2.3. Selection of "Coastal" Grid Points

We compare ζ' at tide gauges and model grid points closest to each tide gauge, in both LR and HR. Grid points are identified using a ball tree algorithm. We do not expect CESM to represent riverine processes in upriver tide gauges, and thus only compare model output to ζ' at tide gauges that are less than 20 km from the nearest HR ocean grid point (resulting in 322 unique comparisons to tide gauge data). The location of tide gauges, and corresponding model grid points, is shown in Figure 1 along a representative coastline (the US east coast). To assess resolution differences at coastal locations without tide gauge records, we perform identical analyses for model output closest to 805 "pseudo-tide gauge" locations spaced approximately every 250 km along global coastlines.

2.4. Altimetry

We use a 1/6° gridded satellite altimetry product (MEaSUREs, 2022), at monthly temporal resolution over the 1993–2018 period, to assess the large-scale spatial structure of ζ' variability. IBE is already removed from this data set; we subtract the same global mean sea level timeseries removed from tide gauge records, and linearly detrend the residual at each gridpoint.

2.5. Filtering Time Series

Temporal variability in ζ' (Figure 2b) is complex, with many superimposed timescales, including long-term trends, decadal anomalies, a strong seasonal cycle, and interannual and subannual variability. Here our focus is on annual and longer timescales over the altimeter record. Other frequency bands are of interest, but are not considered here. In order to isolate these lower frequencies, we first remove the mean seasonal cycle, and apply a 13 months low-pass, fifth order, Butterworth filter to all tide gauge, model, and altimetry ζ' timeseries. We analyze the low-pass filtered timeseries $\left(\zeta'_{LF}\right)$: Figure 2e shows this component at the Charleston tide gauge, with the residual $\left(\zeta'_{HF}\right)$ shown in Figure 2d. ζ'_{LF} timeseries for all tide gauges, and cycle 3 of HR and LR, are shown in Supplementary Figures S3–S6 in Supporting Information S1.

2.6. Partitioning Forced and Intrinsic Variability

We estimate the variance associated with forced and intrinsic sea level variability using inter-cycle differences. For each FOSI cycle n, the total sea level (ζ) time series at each grid point consists of a forced (f) and intrinsic (i) component:

$$\zeta_n(x,y,t) = \zeta_n(t) = \zeta_n^f(t) + \zeta_n^i(t) \tag{1}$$

The difference between any two cycles removes the forced component (and common drift):

$$\zeta^i_{\Delta n}(t) = \zeta^i_{n_1}(t) - \zeta^i_{n_2}(t) \tag{2}$$

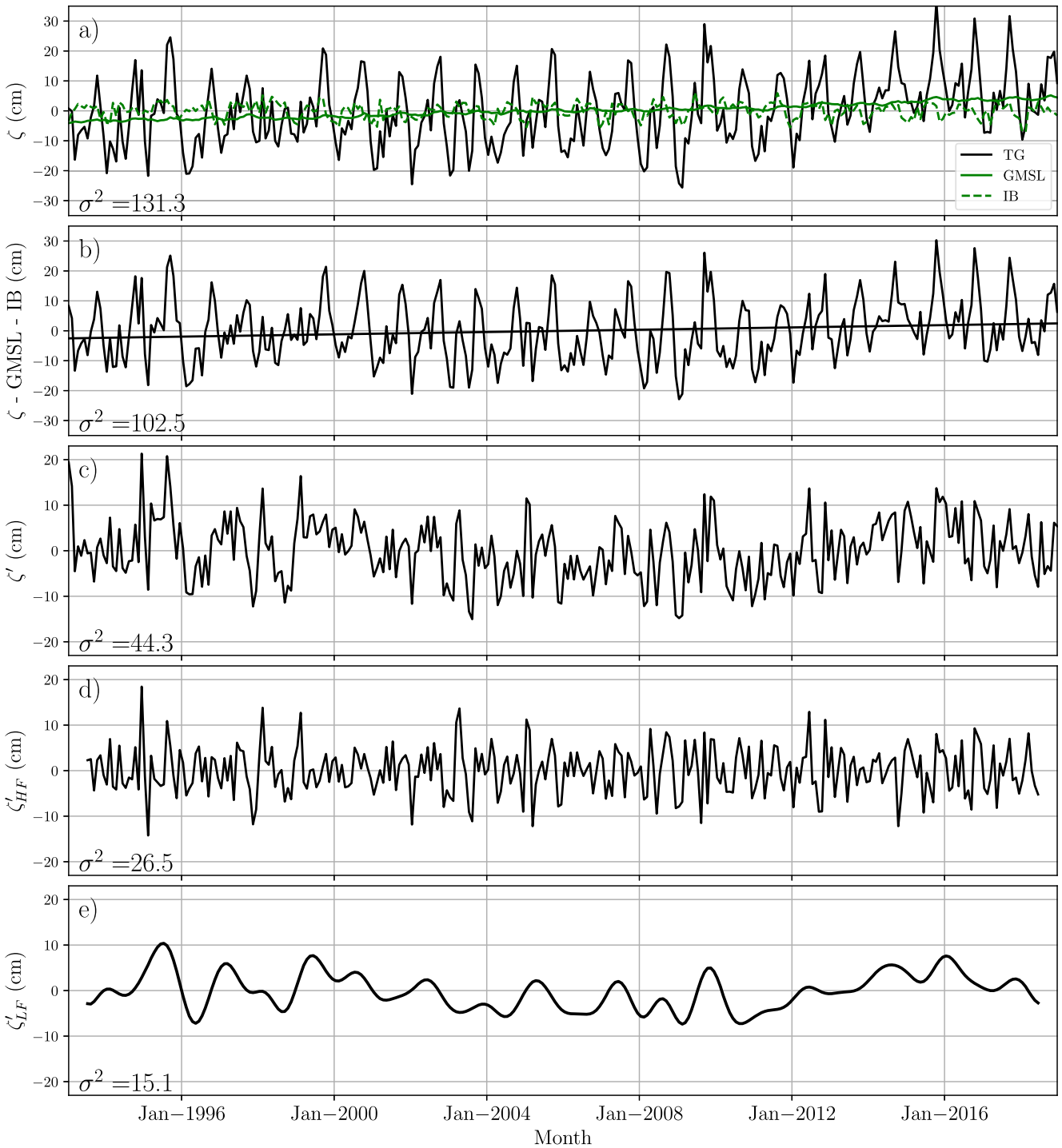

Figure 2. (a) Monthly demeaned relative sea level, in cm, at the Charleston tide gauge (black), global mean sea level (green solid line), and the local contribution from the inverted barometer effect (green dashed line). (b) Relative sea level after removal of the global mean and IBE contribution. Straight black line indicates the linear trend. (c) Relative sea level after removal of the linear trend and climatological seasonal cycle. (d) High pass component (ζ'_{HF}) (e) Low pass component (ζ'_{LF}). Values indicate the variance of each time series.

The variance (σ^2) of the inter-cycle difference is:

$$\sigma^2(\zeta^i_{\Delta n}) = \sigma^2(\zeta^i_{n_1}) + \sigma^2(\zeta^i_{n_2}) + 2 \times \mathrm{Cov}(\zeta^i_{n_1}, \zeta^i_{n_2}) \quad (3)$$

With the assumption that the intrinsic variability in different cycles is uncorrelated (i.e., neglecting the last term in Equation 3), the variance of the differenced time series is equal to the sum of the variance of the intrinsic components of each cycle, for example,:

$$\sigma^2(\zeta^i_{\Delta n_{12}}) \approx \sigma^2(\zeta^i_{n_1}) + \sigma^2(\zeta^i_{n_2}) \quad (4)$$

This assumption has been shown to hold in Close et al. (2020). We can then estimate the variance of the intrinsic component of each cycle by combining equations, for example,:

$$\sigma^2(\zeta^i_{n_1}) \approx 0.5 \times \left[\sigma^2(\zeta^i_{\Delta n_{12}}) + \sigma^2(\zeta^i_{\Delta n_{13}}) - \sigma^2(\zeta^i_{\Delta n_{23}})\right] \quad (5)$$

With four cycles at each resolution, we can calculate two estimates of intrinsic variance for each cycle. Assuming forced and intrinsic variability are uncorrelated, the forced variance is:

$$\sigma^2(\zeta^f_n) \approx \sigma^2(\zeta_n) - \sigma^2(\zeta^i_n) \quad (6)$$

We obtain 8 estimates of intrinsic (σ^2_I) and forced variance at each tide gauge location, for both HR and LR (we do not present partitioned variance for LR, as intrinsic variability is negligible everywhere). In addition, we calculate an additional independent estimate of intrinsic variability using deseasonalized sea level from 26 years of the RYF simulation (see also Penduff et al., 2011). We emphasize that our analysis considers only oceanic intrinsic variability, rather than all internal (unforced) variability in the coupled atmosphere-ocean system.

3. Results

3.1. Comparison of ζ'_{LF} in Tide Gauges and FOSI Simulations

Detrended, deseasonalized, 13-month low-passed coastal sea level (ζ'_{LF}) exhibits considerable spatiotemporal complexity, in both tide gauge sea level records and at coastal gridpoints in FOSI simulations. To highlight our principal findings across a large number of coastal locations (>300), we utilize simplified metrics of observed ζ'_{LF} variability and model-data differences (results are shown in greater detail in Supplementary Figures S3–S6 in Supporting Information S1). Spatial structure is highlighted using two simple, time-independent, aggregate, metrics (variance and correlation), while temporal misfits in spatially coherent alongcoast regions are presented using timeseries from representative locations. These choices are supported by Supplementary Figures S7–S9 in Supporting Information S1: differences between model resolutions, and model-observational misfits (where sufficient tide gauge coverage exists), are similar at $O(10^2-10^3)$ km alongcoast scales, and correspond to well-documented coastal dynamical regimes. Alternate means to assess the spatiotemporal structure of misfits, including spatial averaging and empirical orthogonal functions, were considered but judged unnecessary.

3.1.1. Time-Independent Metrics

The amplitude of observed ζ'_{LF} variability, as measured by its total variance (σ^2_{TG}; Figure 3a), spans approximately two orders of magnitude across global tide gauges, but exhibits clear regional "clusters". For example, σ^2_{TG} is relatively high (over 70 cm^2) in the Baltic seas, with smaller values elsewhere along European coastlines. Similarly, σ^2_{TG} is substantially larger in western Australia than eastern Australia. As noted earlier, the spatial coverage provided by the tide gauge record is quite limited in Africa and the southern hemisphere outside of Australia.

The HR simulation successfully captures the large-scale alongshore structure in ζ'_{LF} variability evident in tide gauges (Figure 3b and Supplementary Figures S3–S9 in Supporting Information S1. However, a normalized metric of HR variance, defined as

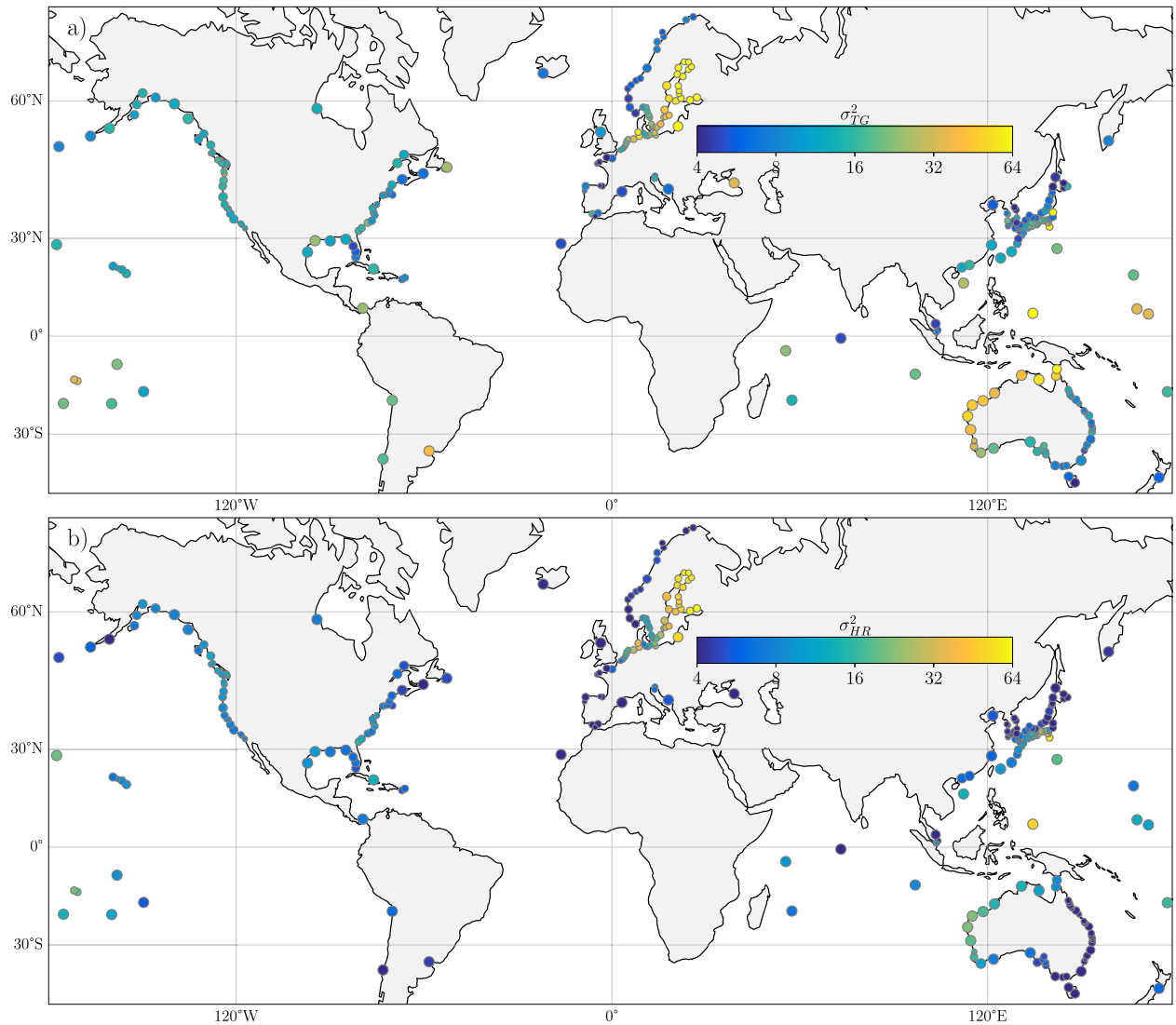

Figure 3. (a) σ^2_{TG}, in cm^2 (note logarithmic color scale), over the 1993–2018 period at 322 global tide gauges. (b) as (a) for HR (σ^2_{HR}; mean across cycle 1–4). To improve the visibility of results at each tide gauge, in this and subsequent figures, the size of points at each tide gauge is scaled by its distance from its nearest neighbor.

$$\overline{R}_{HR} = \frac{1}{4}\sum_{n=1}^{4}\frac{\sigma^2_{HR,n}}{\sigma^2_{TG}} \tag{7}$$

where n is the forcing cycle, highlights differences at global, regional and local scales (Figure 4a). While variance is overestimated at a few tide gauge locations, most prominently in the Kuroshio region, and in narrow channels (e.g., the English Channel and Strait of Gibraltar; see Supplementary Figures S3–S6 in Supporting Information S1 for more detail), variance along coastlines in HR is almost always damped relative to observations. Normalized variance is particularly low throughout the Southern Hemisphere.

At a regional level (e.g., along the western North American coastline), the spatial structure of $\overline{R}_{HR}$ often roughly corresponds to that of σ^2_{TG} (Figure 3a). In these regions, model biases likely relate to the processes that determine the alongcoast extent of regional coastal dynamical regimes. However, there are also regions of underestimated variability (e.g., the entirety of coastal Australia) suggestive of a larger-scale bias (see Figure 9 for supporting evidence, including offshore regions). Some locations, for example, along the United States east coast, exhibit differences suggestive of more localized model errors. These may relate to small-scale unresolved forcing, or

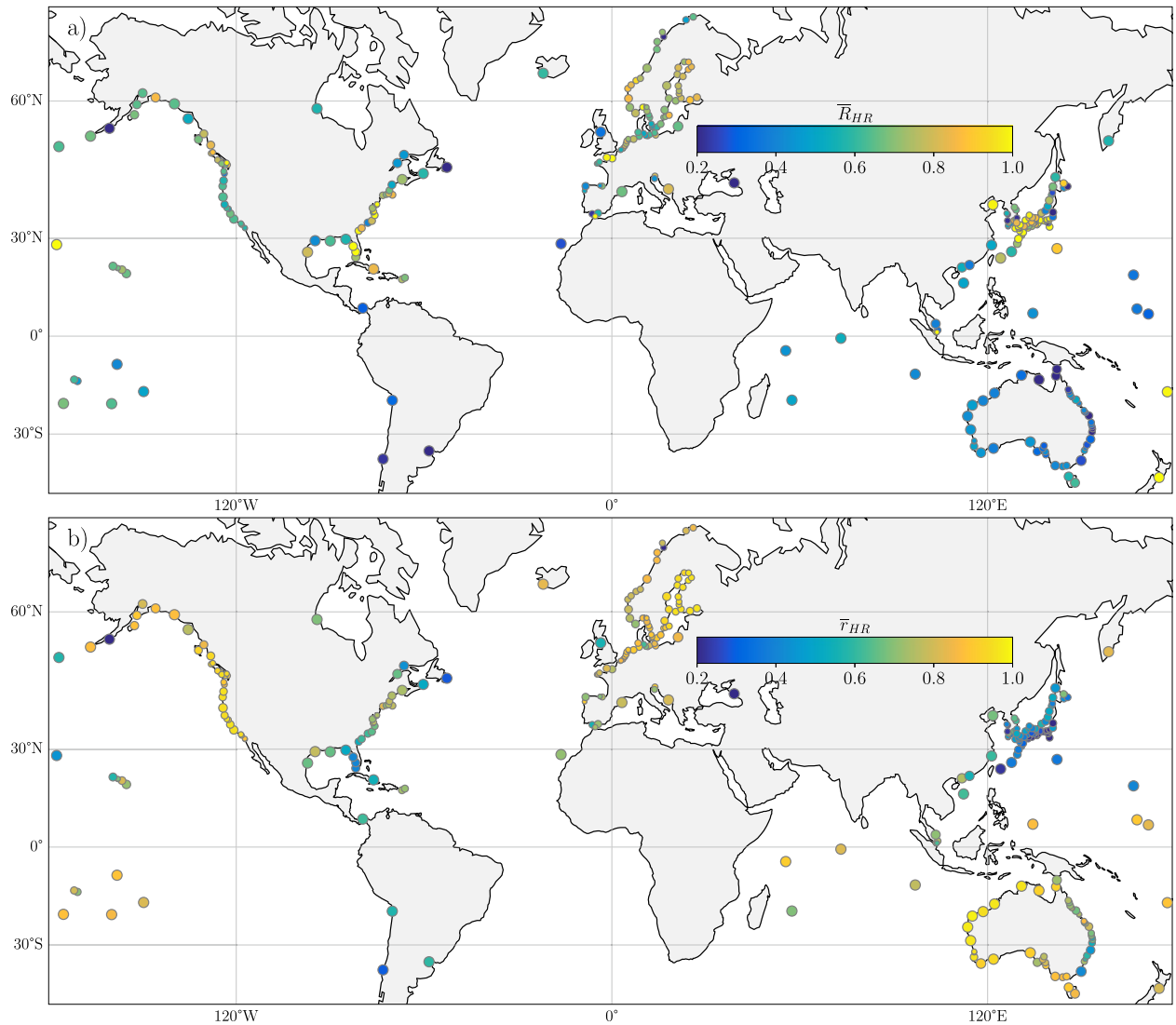

Figure 4. (a) Normalized ζ'_{LF} variance $\left(\overline{R}_{HR}\right)$ in the HR simulations relative to tide gauges. (b) Correlation of ζ'_{LF} in HR and tide gauges $(\overline{r}_{HR})$.

misrepresented coastline and/or bathymetric features. There is also the possibility that some local discrepancies originate in real phenomena, intentionally absent from FOSI simulations, that are not "corrected" by our tide gauge processing (e.g., tectonic effects in Japan).

We use correlation as a simple metric of skill in representing temporal variability against tide gauge observations (Figure 4b). Initially, we consider the mean correlation across four HR cycles, that is,:

$$\overline{r}_{HR} = \frac{1}{4}\sum_{n=1}^{4} r\left(\zeta'^{,HR,n}_{LF}, \zeta'^{,TG}_{LF}\right) \tag{8}$$

Broadly, the spatial structure of $\overline{r}_{HR}$ corresponds well with observed geographic differences in variance. Correlations are fairly high ($\overline{r}_{HR}$> 0.6) in most locations, with values approaching 1.0 on the west coast of the United States, the Baltic Sea, and western Australian coastlines. The lowest values globally (and largest differences between cycles; see Supplementary Figures S3–S6 in Supporting Information S1) are in Japan, especially its eastern coast, with other relatively low correlations along eastern Australia and the US Southeast coast. There is a clear general distinction between oceanic eastern (relatively high correlations) and western (relatively low correlations) boundaries. Local-scale differences are less evident in $\overline{r}_{HR}$ than in $\overline{R}_{HR}$, which may indicate that local

effects predominantly act to amplify or damp regional-scale variability (rather than alter phasing and/or drive qualitatively different variability).

In Figure 5, we compare differences in the representation of the tide gauge record between HR and LR simulations (comparison between LR and tide gauges is shown in Supplementary Figures S10–S11 in Supporting Information S1.) Our discussion again focuses on regional-scale differences between resolutions, beginning with variance (Figure 5a):

$$\overline{\Delta R} = \frac{1}{16}\sum_{m=1}^{4}\sum_{n=1}^{4}\frac{\sigma^2_{HR,m} - \sigma^2_{LR,n}}{\sigma^2_{TG}}, \tag{9}$$

where m and n are the four forcing cycles. Differences in variance in HR and LR are considered significant only if all 16 inter-cycle differences are significant at $p<0.05$ (using a Bartlett's test of homogeneity of variances (Snedecor & Cochran, 1989)).

Because there are very few places in which HR overpredicts variance, positive values of $\overline{\Delta R}$ generally indicate improvements in model representation relative to tide gauges. The largest increases with resolution are in regions in which there is a near-absence of variability in the LR. This is most evident in the Baltic seas, but is also evident in the Adriatic. Substantial (>50%) increases in normalized variance are also seen in western boundary current regions, particularly in locations upstream of boundary current detachment. Near the Baltic Sea, there are regions along the Northern European coast where variance is damped in the HR relative to LR. In most other global locations, normalized variance is similar (e.g., Australia) or slightly increased (<20%) in HR.

We quantify resolution-related differences in correlation using a similar approach:

$$\overline{\Delta r} = \frac{1}{16}\sum_{m=1}^{4}\sum_{n=1}^{4} r\left(\zeta'^{,HR,m}_{LF}, \zeta'^{,TG}_{LF}\right) - r\left(\zeta'^{,LR,n}_{LF}, \zeta'^{,TG}_{LF}\right), \tag{10}$$

Differences in correlation are considered significant if all 16 inter-cycle correlations are significant at $p<0.05$ (using a t-test on correlations after a Fisher Z-transformation (Snedecor & Cochran, 1989)).

Broadly, most locations exhibit moderate increases in correlation with increases in resolution, suggesting improved skill and better process representation in HR. As with variance, there is a dramatic increase in $\overline{\Delta r}$ in marginal seas. Outside of marginal seas, HR exhibits improved correlations over most of Europe. Coastlines adjacent to eastern boundary currents (e.g., western North America and western Australia) exhibit little increase in correlation.

Western boundary currents exhibit a complex response to an increase in ocean model resolution. Most notable are negative values of $\overline{\Delta r}$ in Japan, especially in regions closely bordering the Kuroshio. Other western boundary current regions, including the southeast US and eastern Australia, show a substantial increase in correlation with higher resolution. These results indicate that capturing of additional variance may not lead to enhanced correlation. And conversely, even in locations where there is a strong correlation (e.g., along the western North American coastline), variance may still be substantially underpredicted.

3.1.2. ζ'_{LF} Timeseries at Representative Tide Gauge Locations

In Figure 6, we examine ζ'_{LF} timeseries at a subset of geographically and dynamically diverse locations (noted with black circles in Figure 5). Helsinki (Figures 6a and 6b), along the Baltic Sea coastline, exemplifies the stark differences between HR and LR in marginal seas. The amplitude of HR ζ'_{LF} anomalies is similar to observations, while LR exhibits dramatically damped variability throughout the period. Tregde (Figures 6c and 6d), just outside the Baltic Sea along the Norwegian coast, exhibits higher amplitude variability in LR than HR. However, it is clear that this is too large compared with tide gauge measurements. While HR exhibits misfits in both interannual, and potentially lower-frequency, ζ'_{LF} anomalies, it exhibits a higher correlation with the Tregde tide gauge than LR, and its variance lies much closer to observations.

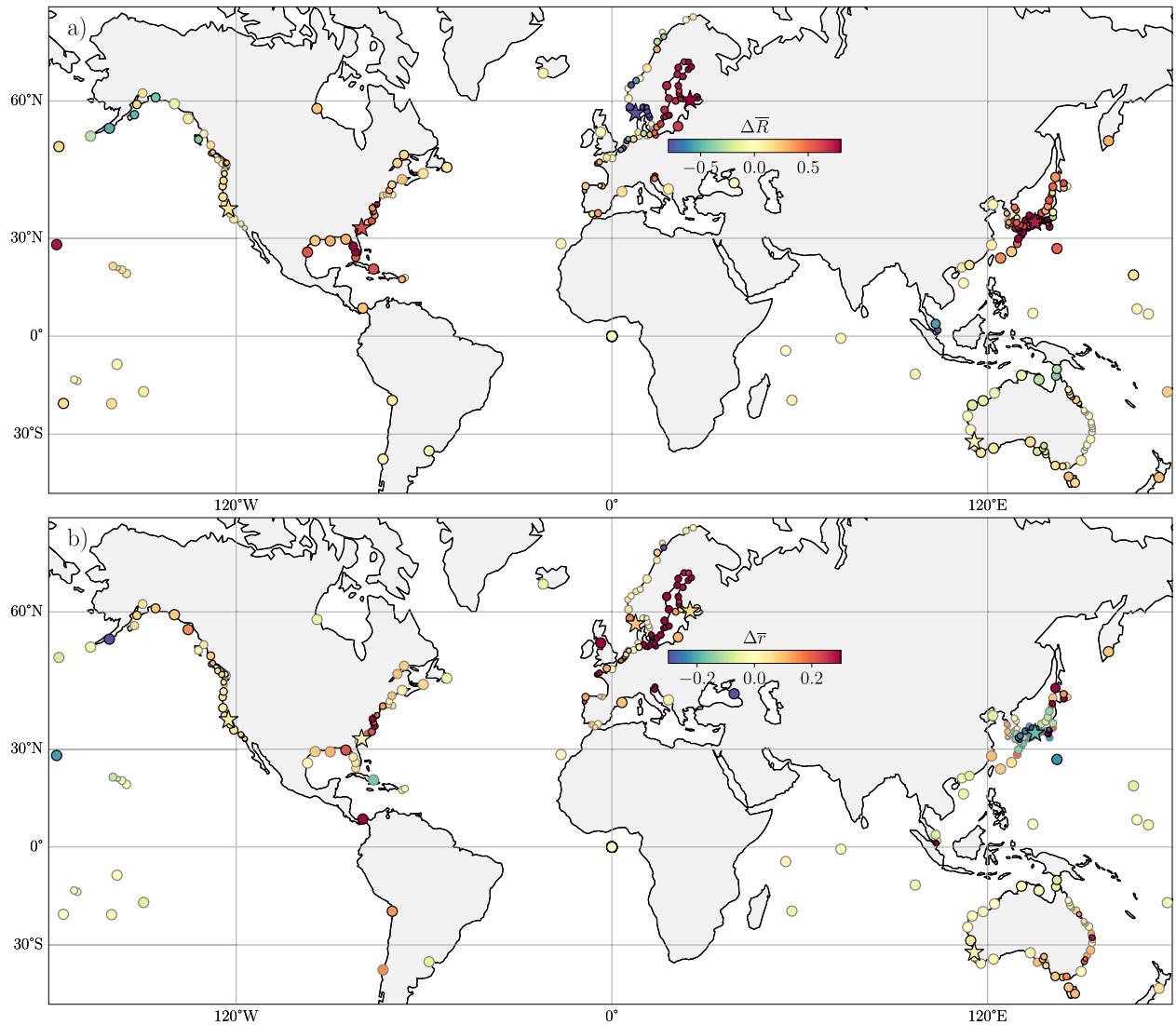

Figure 5. (a) Normalized increase in variance $\left(\overline{\Delta R}\right)$ at each tide gauge. (b) Difference between HR and LR correlation with tide gauge ζ'_{LF} $\left(\overline{\Delta r}\right)$. Black outlined circles indicate the difference between HR and LR is statistically significant. Stars indicate the set of tide gauges for which time series are shown in Figure 6.

In two representative locations adjacent to eastern boundary currents (San Francisco and Fremantle; Figures 6e–6h) the high correlations evident at both resolutions are consistent with very close phase relationships between LR, HR, and tide gauges. There is little obvious dependence on frequency band, with both resolutions showing similar anomalies over annual and interannual-decadal timescales. With respect to amplitude, HR offers only a slight improvement in San Francisco and no improvement in Fremantle.

In contrast, there are dramatic differences in variance between model resolution in two locations near attached western boundary currents (Tan-Nowa, Japan; and Charleston, South Carolina; Figures 6i–6l). Inter-cycle differences in both amplitude and phase clearly suggest a role for intrinsic variability. In these locations, the amplitude of coastal sea level variability observed using tide gauges is far more consistent with HR than LR. At the nearest ocean grid point to Charleston, HR sea level variance is approximately four times that in LR. Correlations, however, exhibit only a limited improvement at Charleston, and are reduced in the mean at Tan-Nowa (in addition to showing a substantial inter-cycle spread). While there are time periods in which HR anomalies common to all cycles follow the tide gauge time series, suggesting a role for an improvement in the representation of forced variability, there are other periods in which there is a substantial spread, or common misfits.

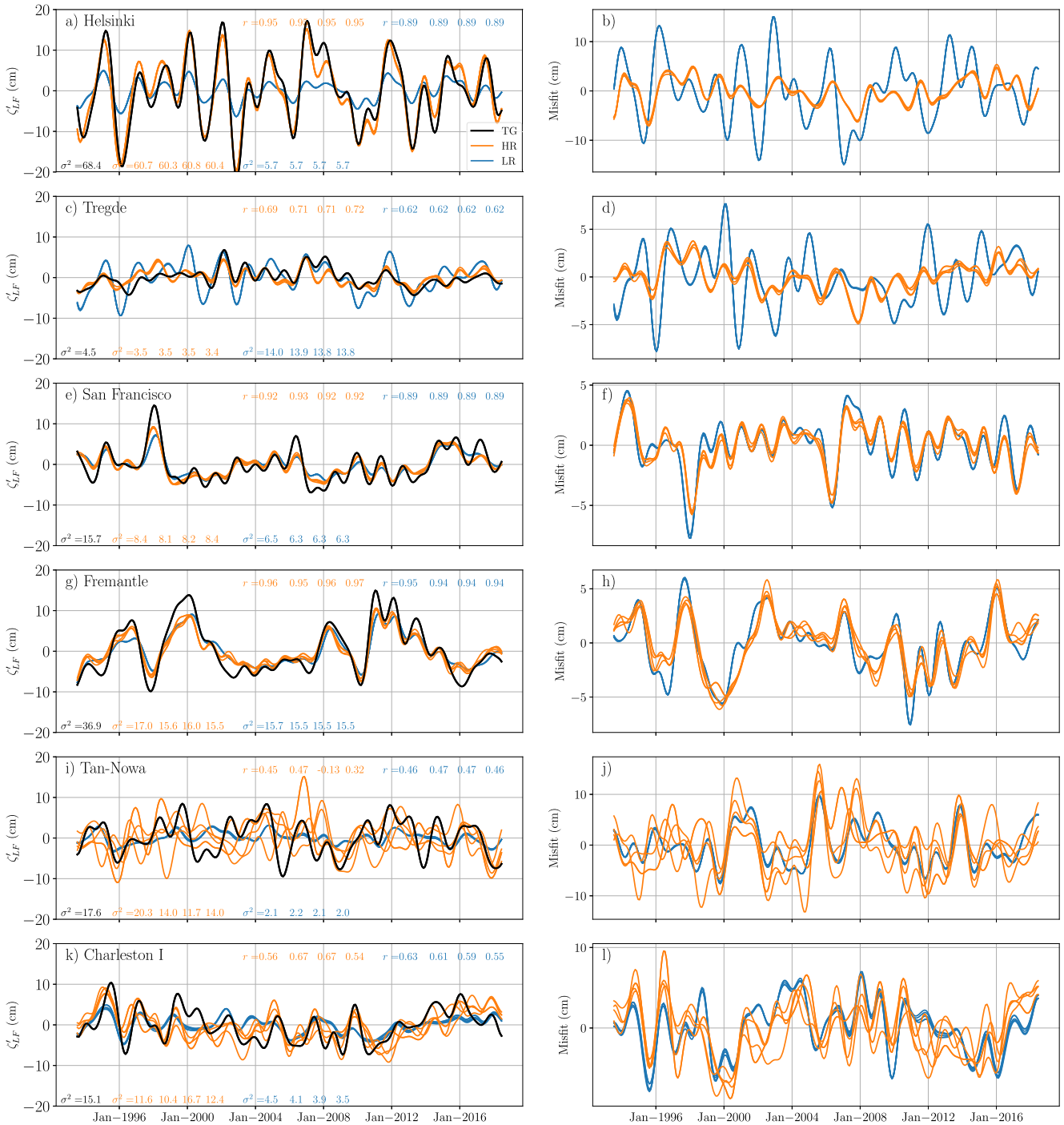

Figure 6. (Left column) ζ'_{LF} for observations (black), LR (blue) and HR (orange) at 6 selected tide gauge locations (noted with black circles in Figure 5). Variance, and correlations with tide gauges, are shown, for each forcing cycle, in each panel. (Right column) Model-observational differences in ζ'_{LF} for LR (blue) and HR (orange). The four lines for LR and HR reflect forcing cycles 1–4.

3.1.3. "Pseudo-Tide Gauge" Comparison

The LR/HR comparison is easily extended to coastal regions that lack tide gauges. As described in methods, we perform such a comparison at approximately uniformly spaced locations ("pseudo-tide gauges") along global coastlines in Figure 7. In this comparison, we calculate the correlation between HR and LR cycles, rather than differences in the correlation with tide gauges.

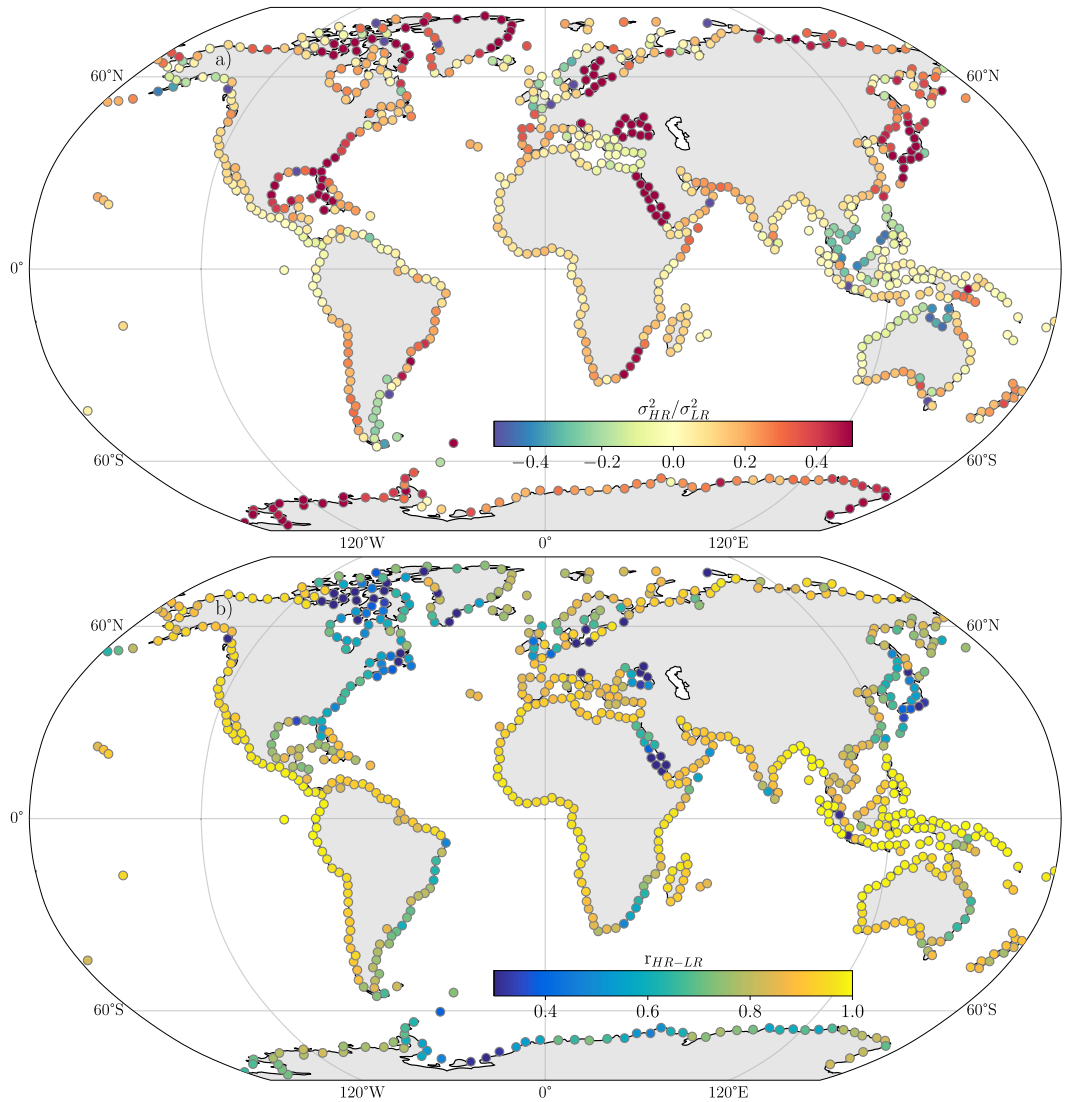

Figure 7. Resolution-sensitivity at 805 pseudo-tide gauge locations. (a) Ratio of the variance in LR to the variance in HR $\left(\frac{\sigma^2_{HR}}{\sigma^2_{LR}}\right)$ at each tide gauge (mean value across cycle 1–4; shown using a $\log_{10}$ scale). (b) Correlation between HR and LR (mean value across 16 pairs of cycles).

Where nearby tide gauges exist, these results more fully define the spatial extent of the regimes identified earlier. For example, the large increase in variance in the Gulf of Mexico and Southeast US in HR is confined to those regions and does not extend further southward along Central and South American coastlines. Along the Southeast US coast, there are stark differences in the variance and correlation at locations to the east (e.g., Bahamas) and west (the US mainland) of the Florida Current.

The limited sensitivity to resolution along the eastern boundaries of the South Atlantic and the entire eastern Pacific margin support a generalization of findings in eastern boundary current regions. Similarly, dramatically enhanced variability in marginal seas is evident in many unmonitored locations (e.g., the Red and Black Sea), extending into narrow regions of complex topography in the Arctic. All regions of attached western boundary currents exhibit large increases in variance in HR, and low correlation between resolutions, perhaps most clearly in the Agulhas current. Coastal regions downstream of subtropical western boundary currents detachments exhibit substantial differences between simulations. For example, relatively low correlations extend well beyond the northern boundary of the Gulf Stream, and variance is not as high. Higher variance along Antarctica, and New Zealand and south Australia suggests that small-scale variability in the Southern Ocean is important in these regions.

3.2. Interpretation of Resolution-Sensitivity and Model-Data Misfits

Collectively, our results highlight dramatic differences in the fidelity and resolution-sensitivity of simulated ζ'_{LF} across coastal dynamical regimes: marginal seas, and eastern and western boundary current regions, comprise the most prominent archetypes.

In marginal seas, large increases in variance, and $\overline{\Delta r}$ where tide gauges exist, are likely due to the improved representation of atmospherically forced volume transport across narrow straits, and improved representation of small-scale bathymetric features. These straits (generally below the grid-scale of coarse resolution models), and the dynamics governing such exchanges, must be resolved in order to capture sea level variability along marginal sea coastlines. Coarse resolution models approximate such unresolved bathymetric and coastline features; the dramatic underestimation of variance in LR in all marginal seas (e.g., near Helsinki; Figure 6a), indicates that, in CESM, these approximations act to limit exchange. Despite identical forcing in the HR simulations, these misfits are largely eliminated once straits are resolved on the model grid. Poor representation of the ocean domain and/or dynamics in marginal seas may also result in errors along open ocean coastlines. For example, sea level variance along the Norwegian coast in LR (Figure 6c), is far larger than observed. This error likely relates to under-estimated energy flux into the (very shallow) Baltic Sea in LR, that, in turn, influences alongcoast energy propagation toward Northern Europe.

Coastlines near attached western boundary currents exhibit dramatic increases in variability in HR, as well as a substantial inter-cycle spread. These results are driven by the ability of HR to represent intrinsic processes in energetic regions, and they are consistent with studies using large ensembles of eddy-permitting, but lower resolution, ocean models (Carret et al., 2021; Close et al., 2020; Sérazin et al., 2015). However, there are marked differences in $\overline{\Delta r}$ and $\overline{\Delta R}$ near different western boundary currents. For example, $\overline{\Delta R}$ is larger, and $\overline{\Delta r}$ is smaller, in coastal locations adjacent to the Kuroshio Current relative to locations near the Gulf Stream, suggesting that a larger fraction of ζ'_{LF} variance arises from intrinsic variability.

Using the HR "ensemble of opportunity", we assess the relative importance of intrinsic variance $\left(\sigma_I^2\right)$ to ζ'_{LF} variability, at each tide gauge location, following the approach described in Section 2.6 (Figure 8). Both the FOSI and RYF simulations reveal that there are many regions of the global coastline in which σ_I^2 is negligible; the only large, continuous, monitored, coastlines where it comprises >5% of total variance occur in Japan, the Southeast US (including the Gulf of Mexico coast), and the eastern coast of Australia (Figures 8a and 8b). Within these regions, the mean ratio of intrinsic to total variance calculated from FOSI inter-cycle differences varies widely, ranging from approximately 0.3 (Southeast US/Australia) to over 0.8 (Japan) (Figure 8a), consistent with the low correlations between HR and TG near the Kuroshio. The RYF simulation provides a very similar estimate of σ_I^2, with respect to both local magnitude and spatial distribution (Figure 8b). While FOSI and RYF estimates show uncertainty on the order of 30% (Figure S12 in Supporting Information S1), differences in the mean value between regions are much larger, indicating significant regional differences in the amplitude and importance of intrinsic variability (as represented in HR simulations). Despite the relatively small number of HR simulations, both the amplitude and spatial structure of intrinsic variance are in close agreement with large (50-member) ensembles (Carret et al., 2021, their Figure 3). In particular, near-coast intrinsic variance is smaller in the Southeast United States than Southeast Japan. Consistency with these earlier studies further strengthens the robustness of our conclusions based on this "ensemble of opportunity".

These estimates of σ_I^2 are consistent with analysis of HR cycle-mean timeseries (Figure 8c), which would be expected to reduce "noise" resulting from unphased intrinsic variability. While correlations remain lower than LR in the Kuroshio region, they are enhanced relative to individual HR forcing cycles, indicating that the reduction in unphased variability improves correlations with the forced component of the observed record. It is possible that, with an ensemble average over more simulations, correlations would be larger than LR. However, robustly isolating "forced" variability and/or resolving time- and/or state-dependence will require a much larger ensemble, or more sophisticated analysis techniques.

In contrast to western boundary current regions, inter-cycle differences in LR and HR time series near eastern boundary currents are very small, and the two order-of-magnitude increase in (areal) resolution generally results in minimal changes to variability (Figure 5). Relatively high correlations suggest that the model is (correctly) simulating a lack of ocean intrinsic variability in observations, but that forced sea level variability is

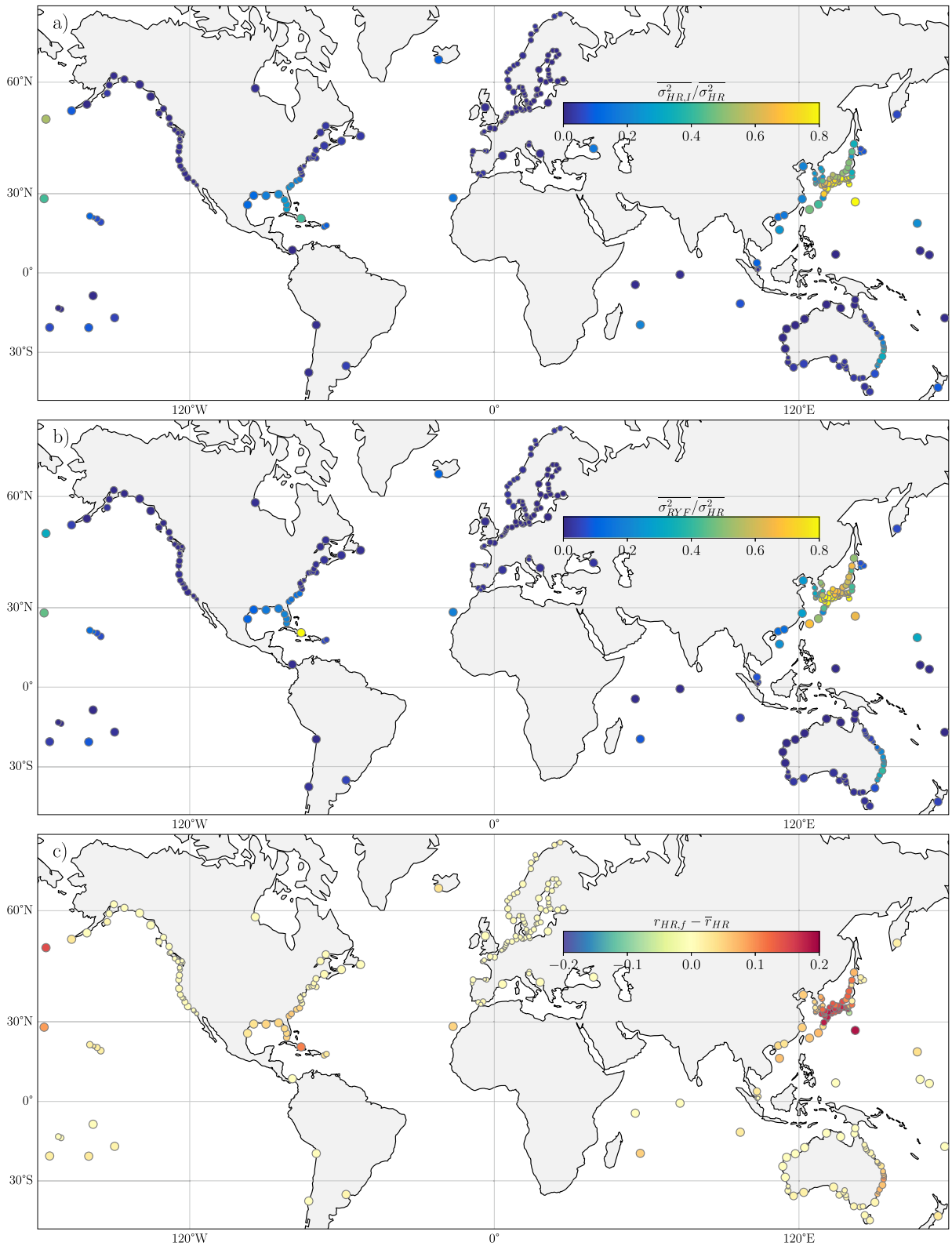

Figure 8. (a) Ratio of intrinsic to total variance in FOSI HR (mean estimate). (b) RYF variance. (c) The difference in correlation with tide gauges when a four-cycle average HR timeseries is used, rather than a mean correlation of four cycles.

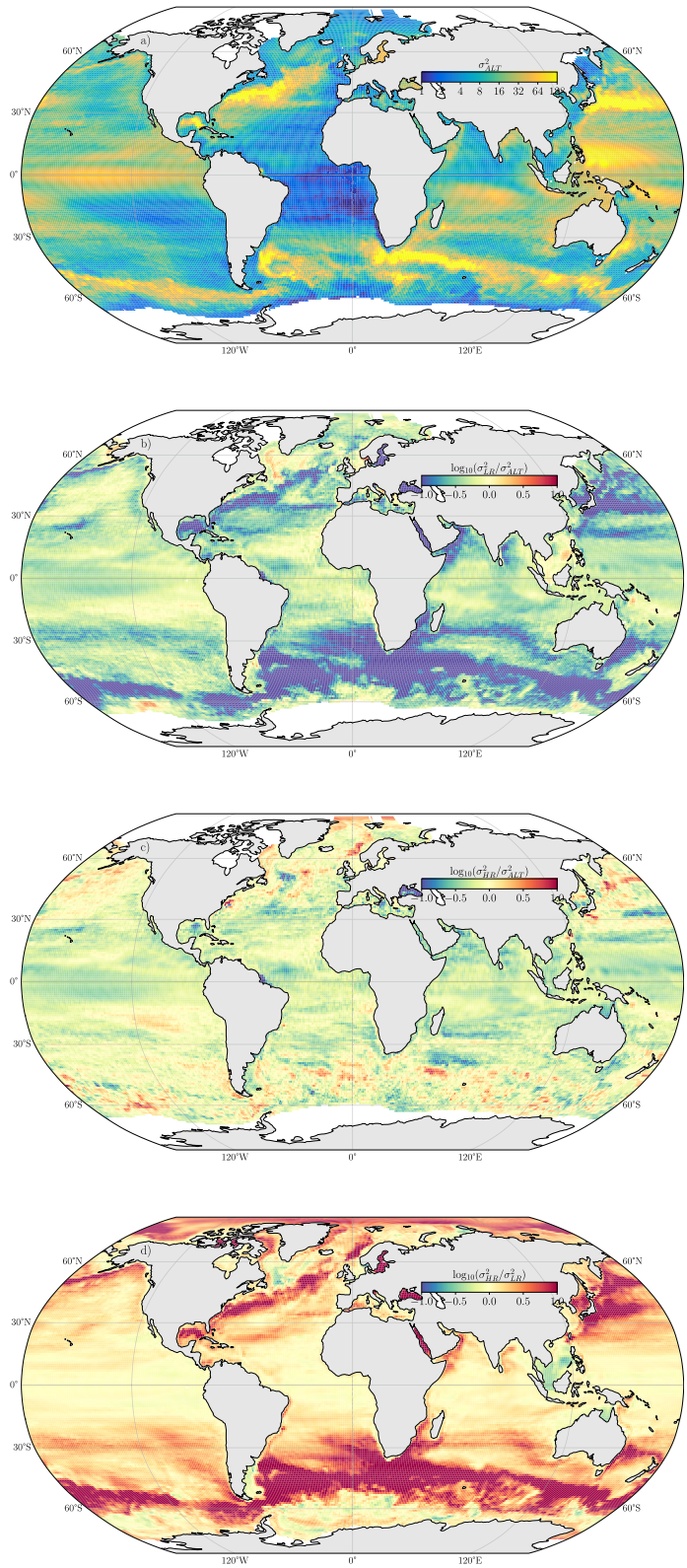

Figure 9. (a) Variance (cm^2, note logarithmic color scale) in ζ'_{LF} over the 1993–2018 period from altimetry. (b) Ratio of ζ'_{LF} variance in LR to altimetry. (c) Ratio of ζ'_{LF} variance in HR to altimetry. (d) Ratio of ζ'_{LF} variance in HR to LR. All monthly time series have been area-averaged to a uniform $\sim 1°$ grid. In (b)–(d), ratios are shown using a $\log_{10}$ scale.

underestimated. The fact that both model resolutions underestimate (presumably forced) coastal sea level variance leaves three possible explanations: (a) variability is underestimated in imposed forcing fields; (b) a weak oceanic response to imposed surface forcing (e.g., due to excessive viscosity, lateral, and/or bottom drag, or an absence of ocean-atmosphere coupling) persists across resolutions; or 3) the relevant across-shelf scales of sea level variability remain unresolved, even at 0.1° resolution.

While each of these explanations may influence regional and local scale misfits, we look for more general, large-scale, insight by comparing ζ'_{LF} variance with satellite altimetry on a common 1° horizontal grid (Figure 9). In regions of high variability, including western boundary currents, the Southern Ocean, and the Arctic, HR exhibits substantially larger ζ'_{LF} variability than LR (Figure 9d). These regions of amplified variance are consistent with those observed in the open ocean (Figure 9a, noting a lack of observations in the Arctic), and our analyses of coastal sea level on well-monitored coastlines near western boundary currents (with the exception of southeast Australia).

However, improvements in the amplitude of variability in HR are primarily located in the extratropics. There is a substantial (∼50%) underestimation of variance, common across both LR and HR, over much of the tropical ocean (Figures 9b and 9c). Such tropical variability is likely to be dynamically connected, through equatorial and coastal waveguides, to the US west coast, Australia, and many other coastal regions. This, in turn, suggests that missing coastal variability may not be related to local forcing (e.g., alongshore winds), but could be due to large scale deficiencies in either the forcing fields, or the ocean response to forcing. The origin of this large-scale underestimation of ζ'_{LF} variance, including its commonality across different ocean models forced with JRA55-do, or other OMIP-style, forcing (Chassignet et al., 2020), deserves further investigation.

4. Discussion

Our global analysis of CESM forced ocean-sea ice (FOSI) simulations indicates that the representation of detrended, 13-month low pass filtered coastal dynamic sea level $\left(\zeta'_{LF}\right)$ variability often—but not always—differs substantially between high (∼0.1°) and low (∼1°) ocean model resolutions. Resolution-sensitivity has been highlighted in prior, more regionally focused, studies, but comparison of global, multi-cycle, FOSI simulations more clearly isolates the influence of ocean model resolution and intrinsic variability across different geographic regions.

This assessment could be extended through comparison of different ocean models (Griffies et al., 2016; Haarsma et al., 2016), or the inclusion of additional observational data sets. For example, long tide gauge records could be used to identify model-data differences in lower-frequency coastal sea level variability. Such an investigation is of merit, but it would have to assess tradeoffs between spatial and temporal coverage of the tide gauge data set. Analysis of longer time periods will also require additional care in the treatment of model drift, nonlinearities in the tide gauge record arising from vertical land motion and solid-earth effects, and uncertainties in the partition between individual components of global mean sea level change. While spurious variability associated with the cyclic forcing protocol is likely small for the time period analyzed here (1993–2018), analyses that extend further back in time would likely need to assess alternate ocean model spinup procedures.

Comparison with coastal altimetric observations from 1993 to present could provide additional insight into the spatial structure of model-data differences. However, altimetry records exhibit systematic differences from the tide gauge record (Vinogradov & Ponte, 2011), originating in physical processes and/or observational errors, which complicates the interpretation of inter-product differences. A more complete analysis of differences across coastal altimetric, tide gauge, and ocean model data sets will be pursued in future work.

Despite these limitations, our analysis provides valuable guidance for sea level forecasting efforts. Accurate representation of historical coastal sea level variability implies that an ocean model sufficiently captures: (a) the ocean's response to atmospheric forcing; and (b) the oceanic memory and/or propagation processes that are key elements of predictability (Frederikse et al., 2022; Polkova et al., 2015). Thus, the relatively high correlations between tide gauges and model output over many global coastlines implies that such processes are often well-represented, either in HR only, or in both HR and LR. These processes also influence climate and ocean variability at longer (e.g., decadal-centennial) timescales, providing at least some confidence in the robustness of longer-timescale projections of coastal sea level. This confidence should, however, be tempered by the ability of coupled models to accurately represent, and project, surface forcing fields.

More specifically, forecasting approaches will benefit from an improved understanding of the origin (e.g., forced or intrinsic) and spatiotemporal properties of coastal sea level variability, and the fidelity with which it is represented in dynamical models of different structure and resolution. For example, along the North American west coast, the timing of sea level variability is well-represented, but anomalies are damped. In this and similar regions, forecasts might inflate the variance of coarse-resolution models using a scaling factor based on the observed record. The use of computationally inexpensive coarse resolution models may then permit a more detailed characterization of uncertainty in, for example, atmospheric forcing fields. Near western boundary currents, resolving processes that lead to intrinsic variability improves agreement with observed sea level variance. However, the chaotic nature of such variability, and its dependence upon initial conditions, pose challenges for forecasting strategies: correlations against observations using a single model realization could yield misleadingly low estimates of potential predictability. At a minimum, ocean intrinsic variability should be recognized as a potentially large source of forecast uncertainty in energetic regions, and ensemble approaches should be prioritized. We note that intrinsic sea level variability may have predictability in initialized simulations, with sufficient resolution and accurate initialization of small scales. The potential value of such approaches requires further study.

Finally, predictive skill analyses are often made using FOSI simulations as the "truth" data set. Biases in FOSI simulations may obscure the absolute predictability in the climate system. For example, a larger signal, and more predictability, may exist in locations in which the ζ'_{LF} variability is damped relative to observations. Such biases should be acknowledged in potential skill assessments even if their effect on real-world predictability is difficult to estimate.

Data Availability Statement

Sea level observations analyzed in this study are available from the Permanent Service for Mean Sea Level (Holgate et al., 2013; Permanent Service for Mean Sea Level, 2024) (for tide gauges) and from NASA (MEaSUREs, 2021) (for satellite altimetry). Derived quantities from CESM simulations, and scripts required to generate figures, are archived at Little (2024).

Acknowledgments
C.L. and S.Y. acknowledge support from US National Science Foundation (NSF) OCE-2148507 and NOAA Climate Program Office NA23OAR4310458. P.C. and S.Y. acknowledge support from the National Academies of Science and Engineering Gulf Research Program Grant 2000013283. R.P. acknowledges support from contract 80NM0018D0004 to JPL (NASA Sea Level Change Team). W.K. is supported by the joint U.K.-NERC/U.S.-NSF WISHBONE project (NSF-2040020). NCAR computational resources were used for data and model analysis; NCAR is a major facility sponsored by the NSF under Cooperative Agreement 1852977. We thank the Permanent Service for Mean Sea Level and the developers of the momlevel Python package (https://momlevel.readthedocs.io/en/v0.0.7/). Maps were generated using python 3.8 (http://www.python.org), matplotlib 3.7.3 (https://matplotlib.org/), and cartopy 0.21.1 (https://scitools.org.uk/cartopy).

References

Becker, M., Karpytchev, M., Marcos, M., Jevrejeva, S., & Lennartz-Sassinek, S. (2016). Do climate models reproduce complexity of observed sea level changes? AOGCMs and the Sea Level complexity. *Geophysical Research Letters*, *43*(10), 5176–5184. https://doi.org/10.1002/2016GL068971

Carret, A., Llovel, W., Penduff, T., & Molines, J. (2021). Atmospherically forced and chaotic interannual variability of regional sea level and its components over 1993–2015. *Journal of Geophysical Research: Oceans*, *126*(4), e2020JC017123. https://doi.org/10.1029/2020JC017123

Chaigneau, A. A., Reffray, G., Voldoire, A., & Melet, A. (2022). IBI-CCS: A regional high-resolution model to simulate sea level in western Europe. *Geoscientific Model Development*, *15*(5), 2035–2062. https://doi.org/10.5194/gmd-15-2035-2022

Chang, P., Zhang, S., Danabasoglu, G., Yeager, S. G., Fu, H., Wang, H., et al. (2020). An unprecedented set of high-resolution earth system simulations for understanding multiscale interactions in climate variability and change. *Journal of Advances in Modeling Earth Systems*, *12*(12), e2020MS002298. https://doi.org/10.1029/2020MS002298

Chassignet, E. P., Yeager, S. G., Fox-Kemper, B., Bozec, A., Castruccio, F., Danabasoglu, G., et al. (2020). Impact of horizontal resolution on global ocean–sea ice model simulations based on the experimental protocols of the Ocean Model Intercomparison Project phase 2 (OMIP-2). *Geoscientific Model Development*, *13*(9), 4595–4637. https://doi.org/10.5194/gmd-13-4595-2020

Close, S., Penduff, T., Speich, S., & Molines, J.-M. (2020). A means of estimating the intrinsic and atmospherically-forced contributions to sea surface height variability applied to altimetric observations. *Progress in Oceanography*, *184*, 102314. https://doi.org/10.1016/j.pocean.2020.102314

Cooley, D. S., & Skern-Mauritzen, M. (2022). Ocean and coastal ecosystems and their services. In H. O. Pörtner (Ed.), *Climate change 2022: Impacts, adaptation and vulnerability. Contribution of working group II to the sixth assessment report of the intergovernmental panel on climate change* (pp. 379–550). Cambridge University Press. (Type: Book Section). https://doi.org/10.1017/9781009325844.004.198

Danabasoglu, G., Yeager, S. G., Bailey, D., Behrens, E., Bentsen, M., Bi, D., et al. (2014). North atlantic simulations in coordinated ocean-ice reference experiments phase II (CORE-II). *part i: Mean states*, *73*, 76–107. https://doi.org/10.1016/j.ocemod.2013.10.005

Downes, S. M., Farneti, R., Uotila, P., Griffies, S. M., Marsland, S. J., Bailey, D., et al. (2015). An assessment of southern ocean water masses and sea ice during 1988–2007 in a suite of interannual CORE-II simulations. *Ocean Modelling*, *94*, 67–94. https://doi.org/10.1016/j.ocemod.2015.07.022

Farneti, R., Downes, S. M., Griffies, S. M., Marsland, S. J., Behrens, E., Bentsen, M., et al. (2015). An assessment of antarctic circumpolar current and southern ocean meridional overturning circulation during 1958–2007 in a suite of interannual CORE-II simulations. *Ocean Modelling*, *93*, 84–120. https://doi.org/10.1016/j.ocemod.2015.07.009

Frederikse, T., Lee, T., Wang, O., Kirtman, B., Becker, E., Hamlington, B., et al. (2022). A hybrid dynamical approach for seasonal prediction of sea-level anomalies: A pilot study for Charleston, South Carolina. *Journal of Geophysical Research: Oceans*, *127*(8). https://doi.org/10.1029/2021JC018137

Gill, A. E. (1982). *Atmosphere-Ocean dynamics* (p. 662pp). Academic Press. (bibtex: gill1982).

Gregory, J. M., Griffies, S. M., Hughes, C. W., Lowe, J. A., Church, J. A., Fukimori, I., et al. (2019). Concepts and terminology for Sea Level: Mean, variability and change, both local and global. *Surveys in Geophysics*, *40*(6), 1251–1289. https://doi.org/10.1007/s10712-019-09525-z

Griffies, S. M., Biastoch, A., Böning, C., Bryan, F., Danabasoglu, G., Chassignet, E. P., et al. (2009). Coordinated Ocean-Ice reference experiments (COREs). *Coordinated ocean-ice reference experiments (COREs)*, *26*(1), 1–46. https://doi.org/10.1016/j.ocemod.2008.08.007

Griffies, S. M., Danabasoglu, G., Durack, P. J., Adcroft, A. J., Balaji, V., Böning, C. W., et al. (2016). OMIP contribution to CMIP6: Experimental and diagnostic protocol for the physical component of the Ocean Model intercomparison project. *Geoscientific Model Development*, *9*(9), 3231–3296. https://doi.org/10.5194/gmd-9-3231-2016

Griffies, S. M., Yin, J., Durack, P. J., Goddard, P., Bates, S. C., Behrens, E., et al. (2014). An assessment of global and regional sea level for years 1993–2007 in a suite of interannual CORE-II simulations. *Ocean Modelling*, *78*, 35–89. https://doi.org/10.1016/j.ocemod.2014.03.004

Haarsma, R. J., Roberts, M. J., Vidale, P. L., Senior, C. A., Bellucci, A., Bao, Q., et al. (2016). High resolution model intercomparison project (HighResMIP v1.0) for CMIP6. *Geoscientific Model Development*, *9*(11), 4185–4208. https://doi.org/10.5194/gmd-9-4185-2016

Hallberg, R. (2013). Using a resolution function to regulate parameterizations of oceanic mesoscale eddy effects. *Ocean Modelling*, *72*, 92–103. https://doi.org/10.1016/j.ocemod.2013.08.007

Hermans, T. H. J., Tinker, J., Palmer, M. D., Katsman, C. A., Vermeersen, B. L. A., & Slangen, A. B. A. (2020). Improving sea-level projections on the Northwestern European shelf using dynamical downscaling. *Climate Dynamics*, *54*(3–4), 1987–2011. https://doi.org/10.1007/s00382-019-05104-5

Hersbach, H., Bell, B., Berrisford, P., Hirahara, S., Horányi, A., Muñoz-Sabater, J., et al. (2020). The ERA5 global reanalysis. *Quarterly Journal of the Royal Meteorological Society*, *146*(730), 1999–2049. https://doi.org/10.1002/qj.3803

Holgate, S. J., Matthews, A., Woodworth, P. L., Rickards, L. J., Tamisiea, M. E., Bradshaw, E., et al. (2013). New data systems and products at the permanent Service for Mean Sea Level. *Journal of Coastal Research*, *29*(3), 493–504.

Holt, J., Hyder, P., Ashworth, M., Harle, J., Hewitt, H. T., Liu, H., et al. (2017). Prospects for improving the representation of coastal and shelf seas in global ocean models. *Geoscientific Model Development*, *10*(1), 499–523. https://doi.org/10.5194/gmd-10-499-2017

Hughes, C. W., Fukumori, I., Griffies, S. M., Huthnance, J. M., Minobe, S., Spence, P., et al. (2019). Sea level and the role of coastal trapped waves in mediating the influence of the open ocean on the coast. *Surveys in Geophysics*, *40*(6), 1467–1492. https://doi.org/10.1007/s10712-019-09535-x

Huthnance, J. M. (2004). Ocean-to-shelf signal transmission: A parameter study. *Journal of Geophysical Research*, *109*(C12). https://doi.org/10.1029/2004JC002358

Ilıcak, M., Drange, H., Wang, Q., Gerdes, R., Aksenov, Y., Bailey, D., et al. (2016). An assessment of the arctic ocean in a suite of interannual CORE-II simulations. part III: Hydrography and fluxes. *Ocean Modelling*, *100*, 141–161. https://doi.org/10.1016/j.ocemod.2016.02.004

Kopp, R. E., Hay, C. C., Little, C. M., & Mitrovica, J. X. (2015). Geographic variability of sea-level change. *Current Climate Change Reports*, *1*(3), 192–204. (Publisher: Springer. https://doi.org/10.1007/s40641-015-0015-5

Large, W. G., & Yeager, S. G. (2009). The global climatology of an interannually varying air–sea flux. *data set*, *33*(2), 341–364. https://doi.org/10.1007/s00382-008-0441-3

Li, D., Chang, P., Yeager, S. G., Danabasoglu, G., Castruccio, F. S., Small, J., et al. (2022). The impact of horizontal resolution on projected sea-level rise along US east continental shelf with the community earth system model. *Journal of Advances in Modeling Earth Systems*, *14*(5). https://doi.org/10.1029/2021MS002868

Little, C. M. (2024). Data and plotting scripts for "Influence of ocean model horizontal resolution on the representation of global annual-to-multidecadal coastal sea level variability [Dataset]. *Zenodo*. https://doi.org/10.5281/zenodo.13919220

Little, C. M., Hu, A., Hughes, C. W., McCarthy, G. D., Piecuch, C. G., Ponte, R. M., & Thomas, M. D. (2019). The relationship between U.S. East coast Sea Level and the atlantic meridional overturning circulation: A review. *Journal of Geophysical Research: Oceans*, *124*(9), 6435–6458. https://doi.org/10.1029/2019JC015152

Little, C. M., Piecuch, C. G., & Ponte, R. M. (2017). *On the relationship between the meridional overturning*. (Vol. 122, pp. 4554–4568). Publisher: Wiley Online Library.

Liu, Z.-J., Minobe, S., Sasaki, Y. N., & Terada, M. (2016). Dynamical downscaling of future sea level change in the western North Pacific using ROMS. *Journal of Oceanography*, *72*(6), 905–922. https://doi.org/10.1007/s10872-016-0390-0

Long, X., Widlansky, M. J., Spillman, C. M., Kumar, A., Balmaseda, M., Thompson, P. R., et al. (2021). Seasonal forecasting skill of sea-level anomalies in a multi-model prediction framework. *Journal of Geophysical Research: Oceans*, *126*(6). https://doi.org/10.1029/2020JC017060

MEaSUREs. (2021). Global Mean Sea Level trend from integrated multi-mission ocean altimeters TOPEX/poseidon, Jason-1, OSTM/Jason-2, and Jason-3 version 5.1. *NASA Physical Oceanography DAAC*. https://doi.org/10.5067/GMSLM-TJ151

MEaSUREs. (2022). MEaSUREs gridded sea surface height anomalies version 2205. *NASA Physical Oceanography DAAC*. https://doi.org/10.5067/SLREF-CDRV3

NOAA. (2022). A NOAA capability for coastal flooding and inundation information and services at climate timescales to reduce risk and improve resilience. Retrieved from https://cpo.noaa.gov/Portals/0/Docs/Risk-Teams/NOAA-Coastal-Inundation-at-Climate-Timescales-Whitepaper.pdf

Penduff, T., Juza, M., Barnier, B., Zika, J., Dewar, W. K., Treguier, A.-M., et al. (2011). Sea level expression of intrinsic and forced ocean variabilities at interannual time scales. *Journal of Climate*, *24*(21), 5652–5670. https://doi.org/10.1175/JCLI-D-11-00077.1

Penduff, T., Juza, M., Brodeau, L., Smith, G. C., Barnier, B., Molines, J.-M., et al. (2010). Impact of global ocean model resolution on sea-level variability with emphasis on interannual time scales. *Ocean Science*, *6*(1), 269–284. https://doi.org/10.5194/os-6-269-2010

Permanent Service for Mean Sea Level. (2024). Tide gauge data. Retrieved from https://psmsl.org/data/obtaining/

Polkova, I., Köhl, A., & Stammer, D. (2015). Predictive skill for regional interannual steric Sea Level and mechanisms for predictability. *Journal of Climate*, *28*(18), 7407–7419. https://doi.org/10.1175/JCLI-D-14-00811.1

Roussenov, V. M., Williams, R. G., Hughes, C. W., & Bingham, R. J. (2008). Boundary wave communication of bottom pressure and overturning changes for the North Atlantic. *Journal of Geophysical Research*, *113*(C8). https://doi.org/10.1029/2007JC004501

Saba, V. S., Griffies, S. M., Anderson, W. G., Winton, M., Alexander, M. A., Delworth, T. L., et al. (2016). Enhanced warming of the northwest Atlantic ocean under climate change: Northwest Atlantic enhanced warming. *Journal of Geophysical Research: Oceans*, *121*(1), 118–132. https://doi.org/10.1002/2015JC011346

Sérazin, G., Penduff, T., Grégorio, S., Barnier, B., Molines, J.-M., & Terray, L. (2015). Intrinsic variability of Sea Level from global ocean simulations: Spatiotemporal scales. *Journal of Climate*, *28*(10), 4279–4292. https://doi.org/10.1175/JCLI-D-14-00554.1

Small, R. J., Kurian, J., Chang, P., Xu, G., Tsujino, H., Yeager, S., et al. (2024). Eastern boundary upwelling systems in ocean–sea ice simulations forced by CORE and JRA55-do: Mean state and variability at the surface. *American Meteorological Society*, *37*(9), 2821–2848. https://doi.org/10.1175/JCLI-D-23-0511.1

Snedecor, G., & Cochran, W. (1989). *Statistical methods*. IOWA State University Press. Retrieved from https://books.google.com/books?id=N09SxgEACAAJ

Stewart, K., Kim, W., Urakawa, S., Hogg, A., Yeager, S., Tsujino, H., et al. (2020). JRA55-do-based repeat year forcing datasets for driving ocean–sea-ice models. *Ocean Modelling*, *147*, 101557. https://doi.org/10.1016/j.ocemod.2019.101557

Tinker, J., Palmer, M. D., Copsey, D., Howard, T., Lowe, J. A., & Hermans, T. H. J. (2020). Dynamical downscaling of unforced interannual sea-level variability in the North-West European shelf seas. *Climate Dynamics*, *55*(7–8), 2207–2236. https://doi.org/10.1007/s00382-020-05378-0

Tseng, Y.-h., Lin, H., Chen, H.-c., Thompson, K., Bentsen, M., Böning, C. W., et al. (2016). North and equatorial pacific ocean circulation in the CORE-II hindcast simulations. *Ocean Modelling*, *104*, 143–170. https://doi.org/10.1016/j.ocemod.2016.06.003

Tsujino, H., Urakawa, L. S., Griffies, S. M., Danabasoglu, G., Adcroft, A. J., Amaral, A. E., et al. (2020). Evaluation of global ocean–sea-ice model simulations based on the experimental protocols of the Ocean Model Intercomparison Project phase 2 (OMIP-2). *Geoscientific Model Development*, *13*(8), 3643–3708. https://doi.org/10.5194/gmd-13-3643-2020

Tsujino, H., Urakawa, S., Nakano, H., Small, R. J., Kim, W. M., Yeager, S. G., et al. (2018). JRA-55 based surface dataset for driving ocean–sea-ice models (JRA55-do). *Ocean Modelling*, *130*, 79–139. https://doi.org/10.1016/j.ocemod.2018.07.002

van Westen, R. M., Dijkstra, H. A., van der Boog, C. G., Katsman, C. A., James, R. K., Bouma, T. J., et al. (2020). Ocean model resolution dependence of Caribbean sea-level projections. *Scientific Reports*, *10*(1), 14599. https://doi.org/10.1038/s41598-020-71563-0

Vinogradov, S. V., & Ponte, R. M. (2011). Low-frequency variability in coastal sea level from tide gauges and altimetry. *Journal of Geophysical Research*, *116*(C7). https://doi.org/10.1029/2011JC007034

Wang, Q., Ilicak, M., Gerdes, R., Drange, H., Aksenov, Y., Bailey, D. A., et al. (2016). An assessment of the arctic ocean in a suite of interannual CORE-II simulations. part i: Sea ice and solid freshwater. *Ocean Modelling*, *99*, 110–132. https://doi.org/10.1016/j.ocemod.2015.12.008

Wise, A., Hughes, C. W., & Polton, J. A. (2018). Bathymetric influence on the coastal Sea Level response to ocean gyres at western boundaries. *Journal of Physical Oceanography*, *48*(12), 2949–2964. https://doi.org/10.1175/JPO-D-18-0007.1

Wise, A., Polton, J. A., Hughes, C. W., & Huthnance, J. M. (2020). Idealised modelling of offshore-forced sea level hot spots and boundary waves along the North American East Coast. *Ocean Modelling*, *155*, 101706. https://doi.org/10.1016/j.ocemod.2020.101706

Woodworth, P. L., Melet, A., Marcos, M., Ray, R. D., Wöppelmann, G., Sasaki, Y. N., et al. (2019). Forcing factors affecting Sea Level changes at the coast. *Surveys in Geophysics*, *40*(6), 1351–1397. https://doi.org/10.1007/s10712-019-09531-1

Yeager, S. G., Chang, P., Danabasoglu, G., Rosenbloom, N., Zhang, Q., Castruccio, F. S., et al. (2023). Reduced southern ocean warming enhances global skill and signal-to-noise in an eddy-resolving decadal prediction system. *npj Climate and Atmospheric Science*, *6*(1), 107. https://doi.org/10.1038/s41612-023-00434-y

Yeager, S. G., Danabasoglu, G., Rosenbloom, N. A., Strand, W., Bates, S. C., Meehl, G. A., et al. (2018). Predicting near-term changes in the earth system: A large ensemble of initialized decadal prediction simulations using the community earth system. *model*, *99*(9), 1867–1886. https://doi.org/10.1175/BAMS-D-17-0098.1

Yeager, S. G., Rosenbloom, N., Glanville, A. A., Wu, X., Simpson, I., Li, H., et al. (2022). The seasonal-to-multiyear large ensemble (SMYLE) prediction system using the community earth system. *model version 2*, *15*(16), 6451–6493. https://doi.org/10.5194/gmd-15-6451-2022

Zhang, Q., Chang, P., Fu, D., Yeager, S. G., Danabasoglu, G., Castruccio, F., & Rosenbloom, N. (2024). Enhanced atlantic meridional mode predictability in a high-resolution prediction system. *Science Advances*, *10*(31), eado6298. https://doi.org/10.1126/sciadv.ado6298

Zhang, X., Church, J. A., Monselesan, D., & McInnes, K. L. (2017). Sea level projections for the Australian region in the 21st century: Sea Level Projections for Australia. *Geophysical Research Letters*, *44*(16), 8481–8491. https://doi.org/10.1002/2017GL074176